The Astronomical Journal, 165:244 (8pp), 2023 June https://doi.org/10.3847/1538-3881/accf10

Observing Atmospheric Escape in Sub-Jovian Worlds with JWST

Leonardo A. Dos Santos[1], Munazza K. Alam[2], Néstor Espinoza[1], and Shreyas Vissapragada[3,4]
[1] Space Telescope Science Institute, 3700 San Martin Drive, Baltimore, MD 21218, USA; ldsantos@stsci.edu
[2] Carnegie Earth & Planets Laboratory, 5241 Broad Branch Road NW, Washington, DC 20015, USA
[3] Center for Astrophysics | Harvard & Smithsonian, 60 Garden Street, Cambridge, MA 02138, USA
Received 2023 February 9; revised 2023 March 29; accepted 2023 April 19; published 2023 May 22

Abstract

Hydrodynamic atmospheric escape is considered an important process that shapes the evolution of sub-Jovian exoplanets, particularly those with short orbital periods. The metastable He line in the near-infrared at 1.083 μm is a reliable tracer of atmospheric escape in hot exoplanets, with the advantage of being observable from the ground. However, observing escaping He in sub-Jovian planets has remained challenging due to the systematic effects and telluric contamination present in ground-based data. With the successful launch and operations of JWST, we now have access to extremely stable high-precision near-infrared spectrographs in space. Here we predict the observability of metastable He with JWST in two representative and previously well-studied warm Neptunes, GJ 436 b ($T_{\rm eq} = 687$ K, $R_{\rm p} = 0.37\,R_{\rm J}$) and GJ 1214 b ($T_{\rm eq} = 588$ K, $R_{\rm p} = 0.25\,R_{\rm J}$). Our simulated JWST observations for GJ 436 b demonstrate that a single transit with NIRSpec/G140H is sensitive to mass-loss rates that are two orders of magnitude lower than what is detectable from the ground. Our exercise for GJ 1214 b show that the best configuration to observe the relatively weak outflows of warm Neptunes with JWST is with NIRSpec/G140H, and that NIRSpec/G140M and NIRISS/SOSS are less optimal. Since none of these instrument configurations can spectrally resolve the planetary absorption, we conclude that the 1D isothermal Parker-wind approximation may not be sufficient for interpreting such observations. More sophisticated models are critical for breaking the degeneracy between outflow temperature and mass-loss rate for JWST measurements of metastable He.

Unified Astronomy Thesaurus concepts: Exoplanet atmospheres (487); Extrasolar gaseous planets (2172); Planet hosting stars (1242); Infrared astronomy (786)

1. Introduction

Surveys for transiting exoplanets have revealed two demographic features that are linked to the evolution of exoplanets: the hot Neptune desert (Szabó & Kiss 2011; Beaugé & Nesvorný 2013; Mazeh et al. 2016) and the radius valley (Fulton et al. 2017; Fulton & Petigura 2018). Short-period sub-Jovian exoplanets may rapidly change in size in their early lives due to atmospheric escape driven by a combination of intense high-energy irradiation from their host star (e.g., Lammer et al. 2003; Owen & Wu 2013; Chadney et al. 2015; Owen & Wu 2017; Ionov et al. 2018; Mordasini 2020) and their internal energy residual from formation (Ginzburg et al. 2018; Gupta & Schlichting 2019). Prior to this discovery, hydrodynamic atmospheric escape (or evaporation) had already been predicted for the early solar system planets (Chamberlain 1963; Watson et al. 1981; Hunten et al. 1987), observed in hot Jupiters (Vidal-Madjar 2003; Vidal-Madjar et al. 2004; Fossati et al. 2010; Lecavelier des Etangs et al. 2010), and later in Neptunes as well (Ehrenreich et al. 2015; Bourrier et al. 2018).

Classically, these observations were first carried out with the ultraviolet (UV) capabilities of the Hubble Space Telescope (HST). In these wavelengths, we have access to escaping neutral H through the Lyα line (1216.67 Å), as well as metallic species like C, N, O, Si, Mg, and Fe (e.g., Linsky et al. 2010; Vidal-Madjar et al. 2013; Ballester & Ben-Jaffel 2015; Dos Santos et al. 2019; Sing et al. 2019; García Muñoz et al. 2021). Some of the challenges of these UV observations arise from the relatively lower efficiency of UV detectors compared to optical or infrared (IR) instruments, the lower observable fluxes of cool stars in the UV, interstellar medium absorption, and the fact that HST is the only telescope capable of UV spectroscopy currently available to the community.

With the discovery of metastable He as a reliable tracer for atmospheric escape in the near-IR (Allart et al. 2018; Mansfield et al. 2018; Oklopčić & Hirata 2018; Spake et al. 2018), transit observations at 1.083 μm have been particularly productive and quickly surpassed the number of evaporation detections compared to UV campaigns (see, e.g., Dos Santos 2022; Kirk et al. 2022; Orell-Miquel et al. 2022). The advantage of these observations is clear: accessibility from the ground permits more systematic surveys using narrowband photometry (e.g., Vissapragada et al. 2022b), as well as the opportunity to resolve planetary absorption at high spectral resolution. Some of the disadvantages of this technique, however, include the fact that populating the metastable He state requires relatively high levels of extreme-ultraviolet flux compared to mid-ultraviolet flux, a condition usually satisfied for K-type stars (Oklopčić 2019). Poppenhaeger (2022) also suggested that stellar coronal abundances have an important role in this process.

Nondetections of metastable He in planets that are expected to be evaporating have been a curious and yet unexplored outcome of observational surveys to date (see, e.g., the case of WASP-80 b; Vissapragada et al. 2022b; Fossati et al. 2022). In particular, the warm Neptune GJ 436 b has been found to be

[4] 51 Pegasi b Fellow.

enshrouded in a large cloud of neutral H fed by atmospheric escape using HST (Ehrenreich et al. 2015; Lavie et al. 2017; Dos Santos et al. 2019). But He observations with the CARMENES spectrograph yielded a nondetection of escaping He (Nortmann et al. 2018). The inferred atmospheric escape rate for GJ 436 b based on the HST observations range from $\sim 10^8$ g s^{-1} (Bourrier et al. 2016) to $\sim 10^{10}$ g s^{-1} (Villarreal D'Angelo et al. 2021). In comparison, the escape rates in hot Jupiters are in the order of $\sim 10^{11}$ g s^{-1} (e.g., Erkaev et al. 2015; Salz et al. 2016). Another curious case is that of GJ 1214 b, whose observations with Keck II/NIRSPEC resulted in nondetections (Kasper et al. 2020; Spake et al. 2022), but a transit observed with CARMENES yielded a tentative detection (Orell-Miquel et al. 2022). Other sub-Jovian worlds for which we expected to observe He escape but only nondetections were reported include K2-100 b (Gaidos et al. 2020), AU Mic b (Hirano et al. 2020), HD 97658 b (Kasper et al. 2020), K2-136 c (Gaidos et al. 2021), and the systems V1298 Tau (Vissapragada et al. 2021), GJ 9827 b (Kasper et al. 2020; Carleo et al. 2021), and HD 63433 (Zhang et al. 2022).

With the successful launch and operations of JWST, we now have access to an extremely precise near-IR space telescope that can potentially give us access to observations of escaping He in sub-Jovian worlds. Fu et al. (2022) demonstrated that the NIRISS spectrograph can detect metastable He in the atmosphere of the hot Saturn HAT-P-18 b. This not only confirms the previous detection from ground-based narrowband photometry (Paragas et al. 2021), but also reveals the presence of a potential He tail trailing the planet (similar to the case of WASP-107 b; Spake et al. 2021). Trailing tails can be missed in narrowband photometry because the techniques used to remove systematic effects (see, e.g., Section 3 of Paragas et al. 2021) can also remove the astrophysical signatures of asymmetric transit light curves.

In this manuscript, we place constraints on the detectability of escaping He in exoplanets with JWST. We simulate the outflow of the representative sub-Jovian worlds GJ 436 b and GJ 1214 b, the metastable He radial profile, and their theoretical transmission spectra at infinite resolution. We also constrain the line-spread function of the NIRSpec spectrograph in the G140H and G140M modes, and use this information to predict the observable transmission spectra. We compare the predicted observable signals and assess the constraints on atmospheric escape that these signals can provide. Finally, we assess which instrumental configuration is best for observing metastable He in transiting exoplanets.

This paper has the following structure: in Section 2, we describe the theoretical and instrumental setup used in this exercise. In Section 3, we discuss the results for GJ 436 b and GJ 1214 b, and their interpretation using a one-dimensional Parker-wind model. Section 4 describes our conclusions and recommendations for future observations.

2. Theoretical and Instrumental Setup

There are two instruments available on JWST that are capable of observing the near-IR He line: NIRISS and NIRSpec. The first has a spectral resolving power of $R \sim 650$ at 1.083 μm (wavelength range 0.6–2.8 μm), while the latter can observe at $R \sim 100$, $R \sim 1000$ and $R \sim 2700$, respectively, for the PRISM (0.5–5.0 μm), G140M and G140H modes (0.80–1.27 μm with the F070LP filter; 0.97–1.84 μm with F100LP). Ideally, higher spectral resolution is desired for He observations because resolving the planetary absorption yields stronger constraints on the outflow temperature—which in turn produces a better mass-loss constraint, since this estimate is degenerate with the outflow temperature. However, even for spectrally unresolved observations, it is still possible to obtain useful constraints for the mass-loss rate if we take into account the energetics of the outflow (Vissapragada et al. 2022a; Linssen et al. 2022). For the particular case of GJ 436 ($J_{\rm mag} = 6.9$), the only instrument configuration on JWST that does not result in saturation is G140H; fainter stars, such as GJ 1214, are observable at lower spectral resolutions.

We simulate the planetary outflows for these two warm Neptunes using the open-source Python framework `p-winds` (Dos Santos et al. 2022). This code assumes that the outflow can be simplified to an isothermal Parker-wind model (Parker 1958) where the mass-loss rate, outflow temperature, and H/He number fraction are free parameters (Oklopčić & Hirata 2018; Lampón et al. 2020). We use version 1.3.4,[5] which includes tidal gravity effects (for more details, see Vissapragada et al. 2022b).

For the first exercise, we aim to assess what mass-loss constraints can readily be obtained from JWST observations. We consider the warm Neptune GJ 436 b as a representative case of a planet known to be undergoing atmospheric mass loss at a rate likely too low to be observable from the ground. We assume a substellar escape rate[6] of 10^8 g s^{-1} and an outflow temperature of 2700 K, based on the estimates from Lyα observations (Bourrier et al. 2016; Villarreal D'Angelo et al. 2021).

Since GJ 436 is observable only with NIRSpec/G140H, the second exercise is to simulate observations of GJ 1214 b to test the performance of the NIRSpec/G140M and NIRISS/SOSS modes in comparison with G140H. Theoretical predictions for this planet estimate a substellar mass-loss rate of 1.9×10^{10} g s^{-1} and outflow temperature of 2700 K (Salz et al. 2016); however, observations from the ground ruled out substellar mass-loss rates higher than 2.5×10^8 g s^{-1} in combination with temperatures lower than 3000 K (Kasper et al. 2020; Spake et al. 2022). For the fiducial simulation of GJ 1214 b, we adopt the escape rate and temperature set by these detection limits.

In these exercises, we assume that GJ 436 b and GJ 1214 b have a solar H/He abundance (although we note that their atmospheric compositions have not yet been conclusively constrained by observations). We adopt the spectral energy distribution (SED) of GJ 436 and GJ 1214 measured in the MUSCLES program[7] (France et al. 2016; see Figure 1). Finally, we assume that the baseline transit depth around the metastable He triplet is constant with a value determined by the average of the transit depth, $(R_{\rm p}/R_{\rm s})^2$, calculated from one-dimensional radiative-convection thermochemical equilibrium forward models from the ATMO model grid (Goyal et al. 2019), scaled to the system parameters for these planets. These forward models assume solar metallicities and C/O and moderate cloud coverage ($\alpha_{\rm cloud} = 0.06$). The value of this baseline transit depth does not have a significant impact on the outcomes of our exercises, since the He signal arises from

[5] The code is available at https://github.com/ladsantos/p-winds.

[6] The term substellar is used to refer to the mass-loss rate assuming that the planet is irradiated over 4π sr. This assumption is used in one-dimensional models like `p-winds`. In reality, planets are irradiated over π sr only, and the total mass-loss rate is obtained by dividing the substellar rate by four.

[7] Publicly available in https://archive.stsci.edu/prepds/muscles/.

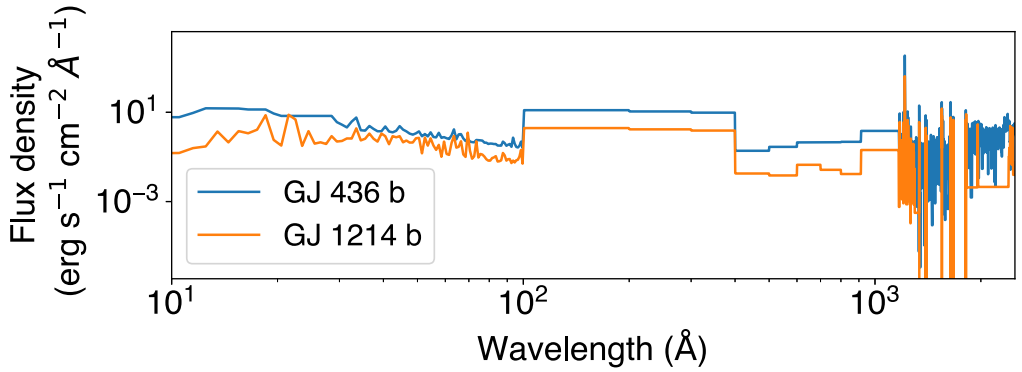

Figure 1. High-energy SED incident on GJ 436 b and GJ 1214 b taken from the MUSCLES database and scaled to the semimajor axis of the planets.

above the planet's thermosphere and is simply added to the transmission spectrum of the lower atmospheric layers.

The final product of the `p-winds` simulation is a theoretical transmission spectrum at infinite spectral resolution. In order to estimate the observable signal, we first need to convolve this theoretical spectrum to the line-spread function (LSF) of the instrument, bin the spectrum to its native wavelength grid, and estimate its uncertainties. For the NIRISS/SOSS LSF, we used the same value used to analyze the He signal in HAT-P-18 b presented in Fu et al. (2022), and which gave good qualitative agreement with the observed signal. For the NIRSpec G140M and G140H modes, we estimated the LSF using an observation from commissioning program PID 1128 (PI: Luetzgendorf)[8]. In particular, we used the FWHM in the cross-dispersion direction of the observations with G140M and G140H in that program as an estimate of the LSF. To perform that measurement, we followed the same procedures described in Espinoza et al. (2023) to estimate the FWHM as a function of wavelength of NIRSpec/G395H. Briefly, the methodology works with the `*rateint.fits` JWST pipeline products, which are median combined, and with which the FWHM is estimated at each column of the spectra under study. Because the spectra are highly tilted and undersampled, the FWHM varies significantly as a function of wavelength. The underlying, physical FWHM of the instrument/mode is estimated as the lower envelope of this FWHM as a function of wavelength curve.

We simulated a single JWST observation by binning the signal observable with G140H to a grid of wavelengths from the aforementioned commissioning observation and injecting noise based on a PandExo (version 2.0; Batalha et al. 2017) simulation for GJ 436 b. We estimate the significance of the detection by fitting a family of Gaussian profiles using the Markov chain Monte Carlo sampler `emcee` (Foreman-Mackey et al. 2013); the signal-to-noise ratio of the detection is defined as the inferred amplitude of the profile divided by its uncertainty.

3. Results

The resulting outflow structures and He distributions for GJ 436 b and GJ 1214 b are shown in Figure 2, and the predicted transmission spectra at infinite resolution are represented as dashed red curves in Figure 3. The metastable He in-transit absorption is narrower than the instrumental LSF, so the signal is spread over 3–4 pixels and assumes the shape of the LSF (see continuous red curves in Figure 3).

For GJ 436 b, our simulations indicate that, if the planet has a substellar escape rate of 10^{8} g s^{-1} and an outflow temperature of 2700 K, its metastable He signature should be observable with NIRSpec/G140H at 9σ confidence. For a higher outflow temperature of 3000 K, the signature will only be marginally detectable in one transit at $\sim 3\sigma$ confidence (see Appendix). In general, lower mass-loss rates and higher outflow temperatures tend to decrease the detectability of the He signal. Our calculations further show that the in-transit signature is spread over 3–4 pixels. This line broadening is dominated by the instrumental LSF, since the intrinsic broadening of the He signal is narrower than one NIRSpec/G140H pixel (see Figure 3).

We used this simulated transmission spectrum (black symbols in Figure 3) to retrieve the escape rate and outflow temperature of GJ 436 b by fitting a family of `p-winds` models using `emcee`. For this retrieval, we set flat priors for both the substellar mass-loss rate $\log \dot{m}$ and the outflow temperature $\log T$. The temperature lower bound is set to 1700 K, which is the limit where cooler models cannot be calculated due to numerical limitations; this is also just below the 2000 K lower limit required to thermally dissociate H_2 at the base of the wind (Murray-Clay et al. 2009; Salz et al. 2016). The lower limit for the mass-loss rate was set arbitrarily to 10^{7} g s^{-1}. The upper limits for temperature and mass-loss rate were set to 7000 K and 10^{11} g s^{-1}, respectively, by assuming that the outflow is powered by photoionization (see the formulation in Vissapragada et al. 2022a).

Our mock retrieval for GJ 436 b shows that, even at the highest spectral resolution ($R \sim 2700$) of JWST with NIRSpec/G140H, our mass-loss rate estimates are degenerate with the outflow temperature (see Figure 4). This degeneracy occurs when the planetary absorption is not spectrally resolved, and it has been observed in studies using narrowband photometry (e.g., Vissapragada et al. 2022a) and HST/WFC3 (e.g., Mansfield et al. 2018). The reason behind this effect is that the temperature of the outflowing material, which is a free parameter in Parker-wind models, is constrained by measuring the broadening of the planetary absorption. When the absorption is not spectrally resolved, its broadening is dominated by the instrumental LSF, and the temperature remains unconstrained. Since the transit depth is affected by both the outflow temperature and the mass-loss rate of the underlying Parker-wind model, there are many combinations of these two parameters that can fit the observed low-resolution transmission spectrum, hence the degeneracy.

[8] DOI:10.17909/2c5e-dm80.

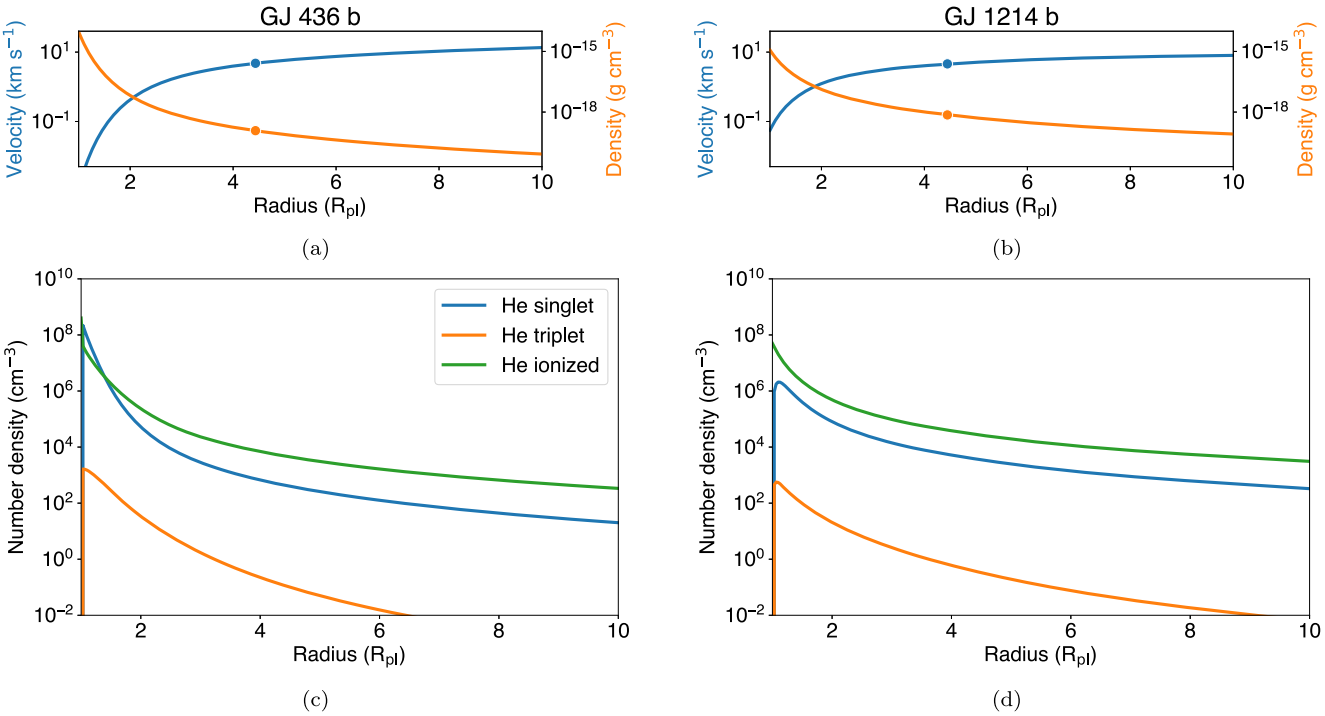

Figure 2. Upper panels: structure of the upper atmosphere of GJ 436 b (left) and GJ 1214 b (right). The circles represent the sonic point of the outflow. Lower panels: distribution of ionized singlet, and triplet He nuclei in the upper atmosphere of GJ 436 b (left) and GJ 1214 b (right).

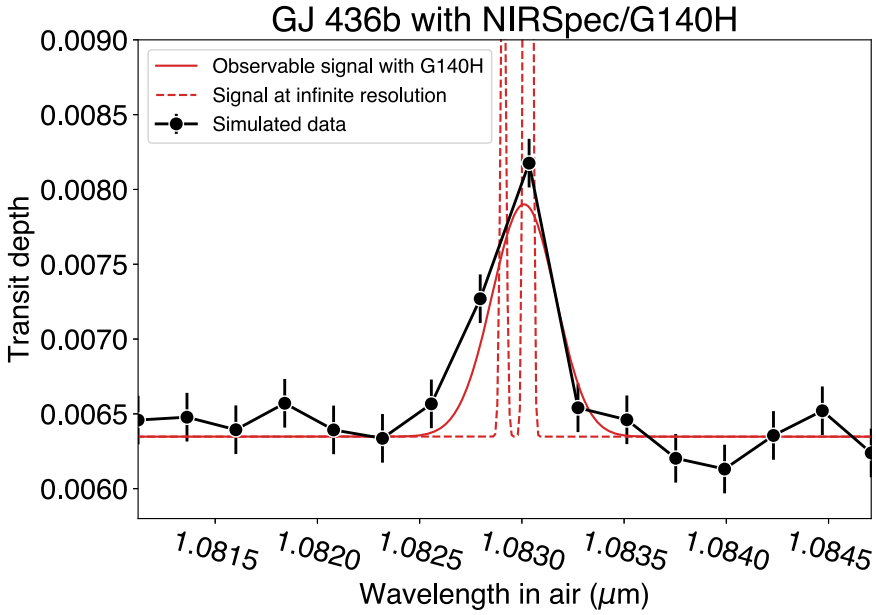

Figure 3. Theoretical (red) and observable (black) metastable He transmission spectra of GJ 436 b assuming a substellar escape rate of 10^8 g s^{-1} and an outflow temperature of 2700 K.

There are different interpretation frameworks that could break this degeneracy. The `p-winds` code has a module that calculates the maximum heating efficiency of a Parker-wind driven by photoionization that sets upper limits to the escape rate and outflow temperature, helping break this degeneracy for hot Jovian exoplanets (see Vissapragada et al. 2022a, 2022b). However, in our simulations we verified that this technique is not very constraining for sub-Jovian worlds at mild levels of irradiation like GJ 436 b and GJ 1214 b. Another technique that aims to limit the parameter space of $\dot{m}$ versus T in unresolved metastable He spectroscopy involves taking into account the effects of radiative heating/cooling, expansion cooling, and heat advection (see Linssen et al. 2022). Ideally, one- or three-dimensional hydrodynamics models (such as the ones described in Salz et al. 2016; Shaikhislamov et al. 2021; Kubyshkina et al. 2022; MacLeod & Oklopčić 2022) break this degeneracy by calculating the outflow temperature profile and mass-loss rates self-consistently, but they are more computationally expensive and they have other free parameters as well —such as atmospheric abundances, stellar wind strength, and planetary magnetic field strength.

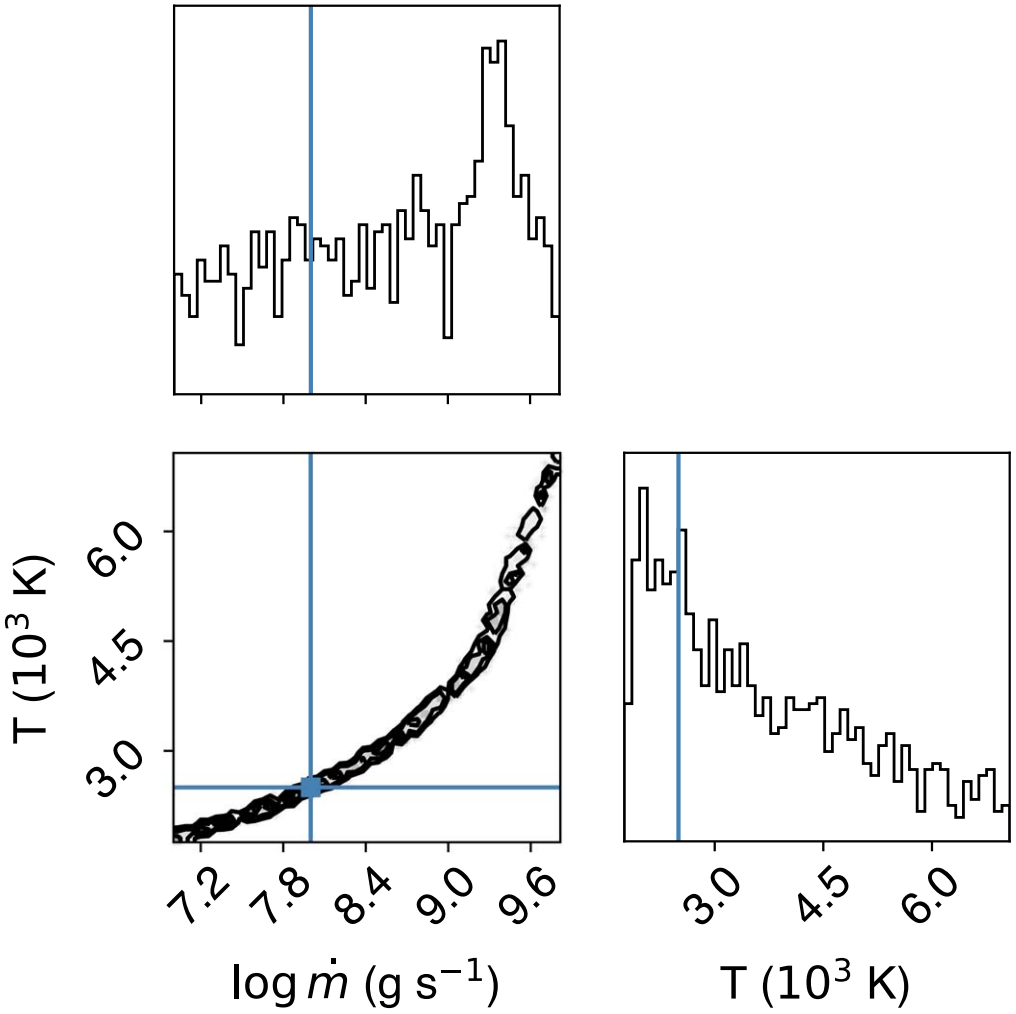

Figure 4. Posterior distributions of substellar mass-loss rate and outflow temperature of GJ 436 b in a mock retrieval with `p-winds`. The injected truth is shown as the blue cross-hair.

Our simulations of the metastable He transmission spectrum of GJ 1214 b show that, for a substellar mass-loss rate of 2.5×10^8 g s^{-1} and outflow temperature of $T = 3000$ K (based on the detection limits of Kasper et al. 2020), the signal is detectable with NIRSpec/G140H at 5σ confidence. The resulting transmission spectra we predict are shown in Figure 5. These simulated data demonstrate that NIRSpec/G140H yields the best-quality metastable He signal compared to NIRSpec/G140M and NIRISS/SOSS, as it would not be detectable in these other two modes (significance of $\sim 2\sigma$ for first and $\sim 1\sigma$ for the second). The trade-off between more precise fluxes and the narrow He signal spreading over a wider wavelength range is not favorable to detect atmospheric escape. This is not the case, however, for hot Jupiters with strong outflows, such as HAT-P-18 b, whose He signal was detected with narrowband photometry (Paragas et al. 2021) and NIRISS/SOSS (Fu et al. 2022). In fact, during our calculations for GJ 1214 b using the mass-loss rate theoretically predicted by Salz et al. (2016), the signal would be readily detectable at high confidence with NIRISS/SOSS (see Appendix).

4. Conclusions and Recommendations

We simulated the transmission spectra of the warm Neptunes GJ 436 b and GJ 1214 b for a single transit with JWST to evaluate the detectability of escaping He and assess how much information we can readily extract from such observations. Our isothermal Parker-wind model of GJ 436 b shows that, for an escape rate of 10^8 g s^{-1}, an outflow temperature of 2700 K, and solar atmospheric abundances, the signal is confidently detected with G140H. Such a shallow signal cannot be observed from the ground, where we have access only to higher mass-loss rates ($\dot{m} \gtrsim 10^{10}$ g s^{-1}). However, the signal size is sensitive to the underlying escape rate and temperature: cooler and stronger outflows are more easily detected, while hotter and weaker outflows are less detectable.

Our exercises demonstrate that observing atmospheric escape in sub-Jovian worlds using the metastable He line will require JWST unless they have strong outflows (see the cases of HAT-P-11 b, GJ 3470b and some young mini-Neptunes; Allart et al. 2018; Palle et al. 2020; Zhang et al. 2023). Weaker outflows are expected in planets with lower-than-solar He abundances, metal-rich atmospheres (Ito & Ikoma 2021; Nakayama et al. 2022), and those whose upper atmospheres are subject to stellar wind confinement (Vidotto & Cleary 2020; MacLeod & Oklopčić 2022).

We generated a simulated transmission spectrum of GJ 436 b with an injected metastable He signal using PandExo. Based on this spectrum, we ran a mock retrieval to estimate the

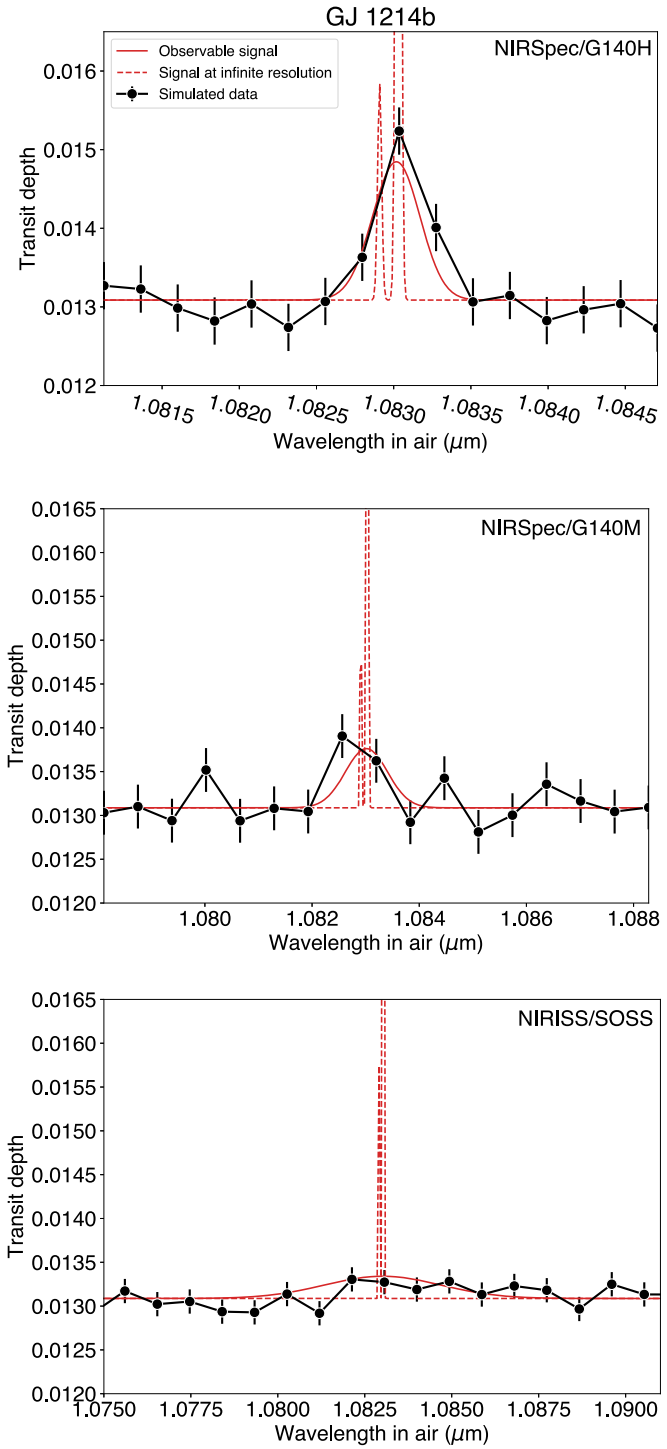

Figure 5. Metastable He transmission spectra of GJ 1214 b simulated for NIRSpec/G140H, G140M and NIRISS/SOSS.

constraints on outflow temperature and mass-loss rate from JWST observations. We found that, since the planetary absorption is not spectrally resolved, there is a degeneracy between the retrieved escape rate and temperature when using an isothermal Parker-wind model.

If we aim to obtain precise constraints on the mass-loss rates of sub-Jovian exoplanets with JWST, it is crucial to use more sophisticated modeling than the 1D isothermal Parker-wind approximation in order to break the degeneracy between outflow temperature and escape rate. Although Vissapragada et al. (2022a) provides a framework to set upper limits by assuming that the outflow is solely powered by photoionization, these upper limits are not as informative for sub-Jovians as they are for hot gas giants. Self-consistent hydrodynamic simulations do not have this degeneracy, since the outflow temperatures and escape rates are set by the underlying physics of the model (e.g., Salz et al. 2016; Shaikhislamov et al. 2021; Kubyshkina et al. 2022). The approach described by Linssen et al. (2022) may also be helpful, as they rule out part of the temperature and mass-loss parameter space by calculating the temperature structure of the outflow based on a self-consistent photoionization model.

Since GJ 436 can be observed only with NIRSpec/G140H due to saturation, we used a similar mock observation of GJ 1214 b to assess whether the NIRSpec/G140M and NIRISS/SOSS modes are viable options to observe metastable He. These other modes are sometimes desirable because they have a wider wavelength coverage, and yield more information about the atmosphere of the planet than the narrower range accessible with NIRSpec/G140H. However, we found that the other modes are less optimal than G140H to detect escaping He, owing mainly to the signal being diluted over several pixels at lower spectral resolution. JWST users wishing to detect atmospheric escape in sub-Jovian worlds should thus use NIRSpec/G140H.

We thank Brett Morris for the coding advice, Nicole Arulanantham for the exchanges about radiative transfer, and the anonymous referee for the helpful review. The `p-winds` code has contributions from Dion Linssen, Lars Klijn, Yassin Jaziri, and Michael Gully-Santiago in the form of finding bugs and improving documentation. This project used archival JWST data openly available in the Mikulski Archive for Space Telescopes (MAST), which is maintained by the Space Telescope Science Institute (STScI). STScI is operated by the Association of Universities for Research in Astronomy, Inc. under NASA contract NAS 5-26555. This research made use of the NASA Exoplanet Archive, which is operated by the California Institute of Technology, under contract with the National Aeronautics and Space Administration under the Exoplanet Exploration Program.

Facilities: JWST(NIRSPec, NIRISS).

Software: NumPy (Harris et al. 2020), SciPy (Virtanen et al. 2020), Astropy (Astropy Collaboration et al. 2018), Jupyter (Kluyver et al. 2016), Matplotlib (Hunter 2007), `emcee` (Foreman-Mackey et al. 2013), `p-winds` (Dos Santos et al. 2022), PandExo (Batalha et al. 2017).

Appendix
Other Simulations of GJ 436 b and GJ 1214 b

We simulated the metastable He signature of GJ 436 b with an escape rate of $\dot{m} = 10^8$ g s^{-1} and an outflow temperature of $T = 3000$ K to illustrate the effect of higher temperatures being less detectable. The resulting transmission spectrum is shown in Figure 6. The signal is only marginally detectable with NIRSpec/G140H with a $\sim 3\sigma$ significance in one transit. However, more transits can be coadded to improve the signal-to-noise ratio of the transmission spectrum.

We also simulated the metastable He signature of GJ 1214 b based on the self-consistent models of Salz et al. (2016), which predict an escape rate of $\dot{m} = 1.9 \times 10^{10}$ g s^{-1} and an outflow temperature of $T = 2700$ K. The resulting transmission spectrum is shown in Figure 7. Due to a significantly higher

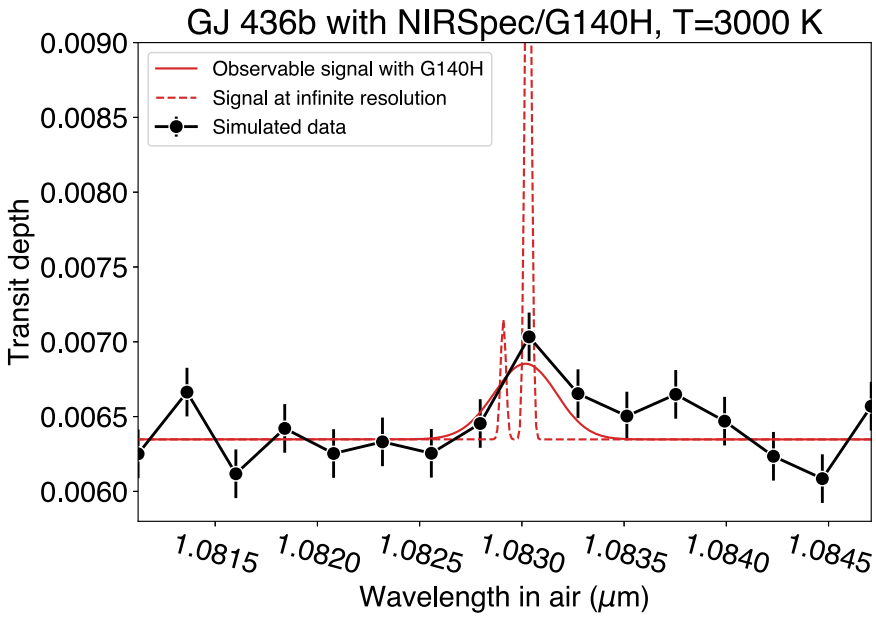

Figure 6. Theoretical (red) and observable (black) metastable He transmission spectra of GJ 436 b assuming a substellar escape rate of 10^8 g s^{-1} and an outflow temperature of 3000 K.

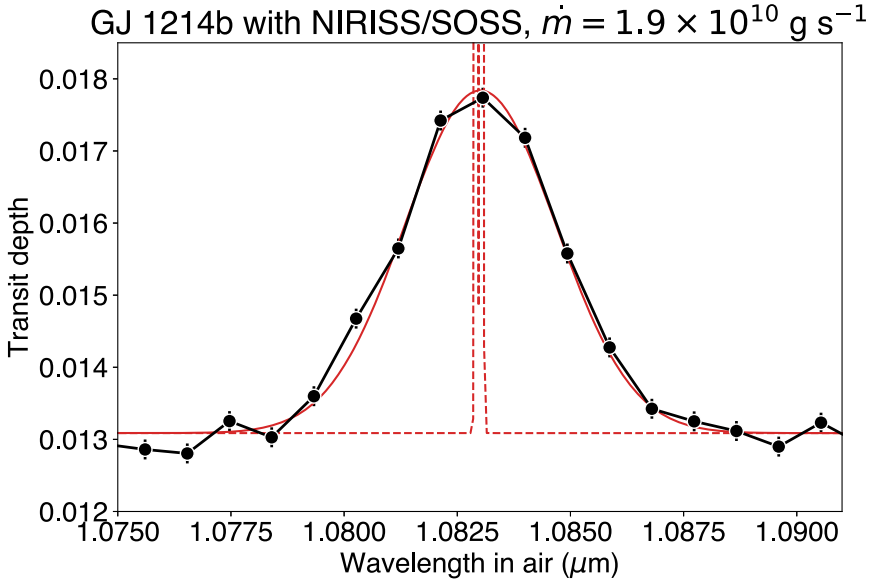

Figure 7. Theoretical (red) and observable (black) metastable He transmission spectra of GJ 1214 b assuming a substellar escape rate of 1.9×10^{10} g s^{-1} and an outflow temperature of 2700 K based on the self-consistent models of Salz et al. (2016).

mass-loss rate, this signal would be readily observable with NIRISS/SOSS and even from ground-based observations. The nondetection obtained by Kasper et al. (2020) with Keck II/NIRSPEC put an upper limit in the mass-loss rate of $\dot{m} < 2.5 \times 10^8$ g s^{-1}.

ORCID iDs

Leonardo A. Dos Santos https://orcid.org/0000-0002-2248-3838
Munazza K. Alam https://orcid.org/0000-0003-4157-832X
Néstor Espinoza https://orcid.org/0000-0001-9513-1449
Shreyas Vissapragada https://orcid.org/0000-0003-2527-1475

References

Allart, R., Bourrier, V., Lovis, C., et al. 2018, Sci, 362, 1384
Astropy Collaboration, Price-Whelan, A. M., Sipőcz, B. M., et al. 2018, AJ, 156, 123
Ballester, G. E., & Ben-Jaffel, L. 2015, ApJ, 804, 116
Batalha, N. E., Mandell, A., Pontoppidan, K., et al. 2017, PASP, 129, 064501
Beaugé, C., & Nesvorný, D. 2013, ApJ, 763, 12
Bourrier, V., Lecavelier des Etangs, A., Ehrenreich, D., et al. 2018, A&A, 620, A147
Bourrier, V., Lecavelier des Etangs, A., Ehrenreich, D., Tanaka, Y. A., & Vidotto, A. A. 2016, A&A, 591, A121
Carleo, I., Youngblood, A., Redfield, S., et al. 2021, AJ, 161, 136
Chadney, J. M., Galand, M., Unruh, Y. C., Koskinen, T. T., & Sanz-Forcada, J. 2015, Icar, 250, 357
Chamberlain, J. W. 1963, P&SS, 11, 901

Dos Santos, L. A. 2022, arXiv:2211.16243
Dos Santos, L. A., Ehrenreich, D., Bourrier, V., et al. 2019, A&A, 629, A47
Dos Santos, L. A., Vidotto, A. A., Vissapragada, S., et al. 2022, A&A, 659, A62
Ehrenreich, D., Bourrier, V., Wheatley, P. J., et al. 2015, Natur, 522, 459
Erkaev, N. V., Lammer, H., Odert, P., Kulikov, Y. N., & Kislyakova, K. G. 2015, MNRAS, 448, 1916
Espinoza, N., Úbeda, L., Birkmann, S. M., et al. 2023, PASP, 135, 018002
Foreman-Mackey, D., Hogg, D. W., Lang, D., & Goodman, J. 2013, PASP, 125, 306
Fossati, L., Guilluy, G., Shaikhislamov, I. F., et al. 2022, A&A, 658, A136
Fossati, L., Haswell, C. A., Froning, C. S., et al. 2010, ApJL, 714, L222
France, K., Loyd, R. O. P., Youngblood, A., et al. 2016, ApJ, 820, 89
Fu, G., Espinoza, N., Sing, D. K., et al. 2022, ApJL, 940, L35
Fulton, B. J., & Petigura, E. A. 2018, AJ, 156, 264
Fulton, B. J., Petigura, E. A., Howard, A. W., et al. 2017, AJ, 154, 109
Gaidos, E., Hirano, T., Mann, A. W., et al. 2020, MNRAS, 495, 650
Gaidos, E., Hirano, T., Omiya, M., et al. 2021, RNAAS, 5, 238
García Muñoz, A., Fossati, L., Youngblood, A., et al. 2021, ApJL, 907, L36
Ginzburg, S., Schlichting, H. E., & Sari, R. 2018, MNRAS, 476, 759
Goyal, J. M., Wakeford, H. R., Mayne, N. J., et al. 2019, MNRAS, 482, 4503
Gupta, A., & Schlichting, H. E. 2019, MNRAS, 487, 24
Harris, C. R., Millman, K. J., van der Walt, S. J., et al. 2020, Natur, 585, 357
Hirano, T., Krishnamurthy, V., Gaidos, E., et al. 2020, ApJL, 899, L13
Hunten, D. M., Pepin, R. O., & Walker, J. C. G. 1987, Icar, 69, 532
Hunter, J. D. 2007, CSE, 9, 90
Ionov, D. E., Pavlyuchenkov, Y. N., & Shematovich, V. I. 2018, MNRAS, 476, 5639
Ito, Y., & Ikoma, M. 2021, MNRAS, 502, 750
Kasper, D., Bean, J. L., Oklopčić, A., et al. 2020, AJ, 160, 258
Kirk, J., Dos Santos, L. A., López-Morales, M., et al. 2022, AJ, 164, 24
Kluyver, T., Ragan-Kelley, B., Pérez, F., et al. 2016, in Positioning and Power in Academic Publishing: Players, Agents and Agendas, ed. F. Loizides & B. Scmidt (Netherlands: IOS Press), 87, https://eprints.soton.ac.uk/403913/
Kubyshkina, D., Vidotto, A. A., Villarreal D'Angelo, C., et al. 2022, MNRAS, 510, 2111
Lammer, H., Selsis, F., Ribas, I., et al. 2003, ApJL, 598, L121
Lampón, M., López-Puertas, M., Lara, L. M., et al. 2020, A&A, 636, A13
Lavie, B., Ehrenreich, D., Bourrier, V., et al. 2017, A&A, 605, L7
Lecavelier des Etangs, A., Ehrenreich, D., Vidal-Madjar, A., et al. 2010, A&A, 514, A72
Linsky, J. L., Yang, H., France, K., et al. 2010, ApJ, 717, 1291
Linssen, D. C., Oklopčić, A., & MacLeod, M. 2022, A&A, 667, A54
MacLeod, M., & Oklopčić, A. 2022, ApJ, 926, 226
Mansfield, M., Bean, J. L., Oklopčić, A., et al. 2018, ApJL, 868, L34
Mazeh, T., Holczer, T., & Faigler, S. 2016, A&A, 589, A75
Mordasini, C. 2020, A&A, 638, A52
Murray-Clay, R. A., Chiang, E. I., & Murray, N. 2009, ApJ, 693, 23
Nakayama, A., Ikoma, M., & Terada, N. 2022, ApJ, 937, 72
Nortmann, L., Pallé, E., Salz, M., et al. 2018, Sci, 362, 1388
Oklopčić, A. 2019, ApJ, 881, 133
Oklopčić, A., & Hirata, C. M. 2018, ApJL, 855, L11
Orell-Miquel, J., Murgas, F., Pallé, E., et al. 2022, A&A, 659, A55
Owen, J. E., & Wu, Y. 2013, ApJ, 775, 105
Owen, J. E., & Wu, Y. 2017, ApJ, 847, 29
Palle, E., Nortmann, L., Casasayas-Barris, N., et al. 2020, A&A, 638, A61
Paragas, K., Vissapragada, S., Knutson, H. A., et al. 2021, ApJL, 909, L10
Parker, E. N. 1958, ApJ, 128, 664
Poppenhaeger, K. 2022, MNRAS, 512, 1751
Salz, M., Czesla, S., Schneider, P. C., & Schmitt, J. H. M. M. 2016, A&A, 586, A75
Shaikhislamov, I. F., Khodachenko, M. L., Lammer, H., et al. 2021, MNRAS, 500, 1404
Sing, D. K., Lavvas, P., Ballester, G. E., et al. 2019, AJ, 158, 91
Spake, J. J., Oklopčić, A., & Hillenbrand, L. A. 2021, AJ, 162, 284
Spake, J. J., Oklopčić, A., Hillenbrand, L. A., et al. 2022, ApJL, 939, L11
Spake, J. J., Sing, D. K., Evans, T. M., et al. 2018, Natur, 557, 68
Szabó, G. M., & Kiss, L. L. 2011, ApJ, 727, L44
Vidal-Madjar, A., Désert, J.-M., Lecavelier des Etangs, A., et al. 2004, ApJL, 604, L69
Vidal-Madjar, A., Huitson, C. M., Bourrier, V., et al. 2013, A&A, 560, A54
Vidal-Madjar, A., Lecavelier des Etangs, A., Désert, J.-M., et al. 2003, Natur, 422, 143
Vidotto, A. A., & Cleary, A. 2020, MNRAS, 494, 2417
Villarreal D'Angelo, C., Vidotto, A. A., Esquivel, A., Hazra, G., & Youngblood, A. 2021, MNRAS, 501, 4383
Virtanen, P., Gommers, R., Oliphant, T. E., et al. 2020, NatMe, 17, 261
Vissapragada, S., Knutson, H. A., dos Santos, L. A., Wang, L., & Dai, F. 2022a, ApJ, 927, 96
Vissapragada, S., Knutson, H. A., Greklek-McKeon, M., et al. 2022b, AJ, 164, 234
Vissapragada, S., Stefánsson, G., Greklek-McKeon, M., et al. 2021, AJ, 162, 222
Watson, A. J., Donahue, T. M., & Walker, J. C. G. 1981, Icar, 48, 150
Zhang, M., Knutson, H. A., Dai, F., et al. 2023, AJ, 165, 62
Zhang, M., Knutson, H. A., Wang, L., et al. 2022, AJ, 163, 68